

Supporting Information

Quantitative analysis of time-resolved RHEED during growth of vertical nanowires

Julian Jakob,^{*ab} Philipp Schroth,^{abc} Ludwig Feigl,^b Daniel Hauck,^b Ullrich
Pietsch,^c and Tilo Baumbach^{ab}

^a *Laboratory for Applications of Synchrotron Radiation, Karlsruhe Institute of
Technology, Kaiserstraße 12, D-76131 Karlsruhe, Germany. E-mail:
julian.jakob@kit.edu*

^b *Institute for Photon Science and Synchrotron Radiation, Karlsruhe Institute of
Technology, Hermann-von-Helmholtz-Platz 1, D-76344 Eggenstein-Leopoldshafen,
Germany.*

^c *Solid State Physics, Emmy-Noether Campus, Walter-Flex Straße 3, D-57068
Siegen, Germany.*

1 NW growth

The NW growth of self-catalysed GaAs NW on Si(111) substrates covered with native oxide was performed in a custom build MBE system [1], which is equipped with a Specs RHD-30 RHEED gun, the diffraction patterns are recorded with a low noise 14-bit PCO PixelFly camera on a fluorescence screen. The RHEED setup was used at 20 keV. Prior loading in the MBE chamber, the substrates were degassed at $T = 300$ °C for 30 min. The actual growth was performed with the so called "surface modification method", presented recently [2]. The first thermal annealing was performed at approximately $T = 750$ °C for 30 min, followed by the first Ga droplet deposition at a certain T with different Ga fluxes for the samples (step 2 in table 1.1) and desorption of the droplets at $T = 750$ °C for 15 min. Now we use an additional Ga droplet deposition step (step 4 in table 1.1), which is different to the original procedure [2], before initiating the NW growth by opening the valve of the arsenic cracker cell. Both last steps are performed at $T = 590$ °C.

Table 1.1: Growth conditions of samples A-F.

Sample	deposited Ga (step 2)	deposited Ga (step 4)	V/III ratio and Ga flux
A	8 ML at $T = 570$ °C	10 ML	2.1 at 0.1 ML/s
B	8 ML at $T = 570$ °C	10 ML	2.1 at 0.1 ML/s
C	4 ML at $T = 570$ °C	10 ML	2.1 at 0.1 ML/s
D	8 ML at $T = 570$ °C	8 ML	2.6 at 0.08 ML/s
E	48 ML at $T = 560$ °C	40 ML	2.1 at 0.1 ML/s
F	48 ML at $T = 540$ °C	40 ML	2.1 at 0.1 ML/s

2 RHEED: experimental data and simulation

After the growth experiments the time-resolved RHEED patterns were processed by a background correction, where we summed up the intensity in the vicinity of each diffraction spot separately ($\Delta q_x = 0.63 \text{ 1/\AA}$, $\Delta q_z = 0.45 \text{ 1/\AA}$). Additionally, we summed up the intensity close to the diffraction spot in the same qz interval and normalized it to equal area as a measure for the background. After this background correction, we additionally correct for the structure factors. The simulation of the data was performed in a separate parameter spaces for each sample, the parameters can be found in table 2.1. Table 2.2 show the whole simulated parameter space, as well as the parameter space resulting in the best description of the experimental data and the parameters extracted by post-growth SEM of samples C and D. The large confidence interval of the NW radii, which all result in a good agreement with the experimental data, originate from the discussed fact that the NW radius has less impact on the RHEED intensity evolution due to self-shadowing. The diffraction signal essentially originates from the edges tip regions of the hexagonal cross section. This means that the ambiguity of the radius results achieved in the simulation needs to be reduced by complementary SEM studies. Table 2.3 shows the simulation parameters and post-growth SEM values for sample E and F. The further parameters for the simulation are for $A = 400 \text{ }\mu\text{m} \cdot 50 \text{ }\mu\text{m}$, for $\alpha = 0.6^\circ$, for $\Lambda = 12 \text{ nm}$, for $K^{obj}(t_f) = 1000$ and for $j = 5$ repetitions. The simulated curves consist of 100 points, the simulated as well as the experimental curves were normalized to equal areas and afterwards the

Table 2.1: List of parameters used in the simulation.

r_0^{NW}	initial NW radius at substrate	t_f	final growth time
$r_{f,b}^{NW}$	final NW radius at substrate	h_f^{NW}	final NW height
$r_{f,t}^{NW}$	final NW radius at tip	$m_{NW,axial} = \frac{h_f^{NW}}{t_f}$	NW axial growth rate
r_0^{cry}	initial crystallite radius	$m_{facet} = \frac{r_{f,b}^{NW} - r_0^{NW}}{t_f}$	NW facet growth rate
r_f^{cry}	final crystallite radius	$m_{tapering} = \frac{r_{f,t}^{NW} - r_{f,b}^{NW}}{t_f}$	NW tapering growth rate
h_0^{cry}	initial crystallite height	$m_{cry,axial} = \frac{h_f^{cry} - h_0^{cry}}{t_f}$	crystallite axial growth rate
h_f^{cry}	final crystallite height	$m_{radial} = \frac{r_f^{cry} - r_0^{cry}}{t_f}$	crystallite radial growth rate

Table 2.2: Parameters used for the simulation of the RHEED integrated intensity and parameters extracted from the post-growth SEM images.

Parameter	Sample C			Sample D		
	simulated interval	Best results of simulation	SEM	simulated interval	Best results of simulation	SEM
ρ_{NW} (μm^{-2})	0.007 - 0.03	$0.01_{-0.002}^{+0.04}$	$0.029_{-0.007}^{+0.007}$	0.07 - 0.4	$0.2_{-0.0}^{+0.1}$	$0.15_{-0.03}^{+0.03}$
r_0^{NW} (nm)	10 - 22	16_{-1}^{+4}	- -	10 - 26	13_{-3}^{+7}	- -
$r_{f,b}^{NW}$ (nm)	18 - 30	18_{-0}^{+5}	19_{-2}^{+2}	13 - 31	23_{-4}^{+1}	21_{-5}^{+5}
$r_{f,t}^{NW}$ (nm)	18 - 30	22_{-4}^{+4}	22_{-2}^{+2}	17 - 35	24_{-4}^{+4}	24_{-2}^{+2}
h_f^{NW} (nm)	800 - 1200	900_{-0}^{+200}	1000_{-10}^{+10}	750 - 1300	1100_{-150}^{+50}	1060_{-20}^{+20}
ρ_{cry} (μm^{-2})	0.6 - 9.0	$0.8_{-0.0}^{+1.2}$	$10.4_{-1.3}^{+1.3}$	0.5 - 5.0	$0.5_{-0.0}^{+0.4}$	$1.0_{-0.3}^{+0.3}$
r_0^{cry} (nm)	10 - 50	15_{-0}^{+15}	- -	15 - 35	15_{-0}^{+20}	- -
r_f^{cry} (nm)	50 - 100	30_{-0}^{+20}	40_{-6}^{+6}	80 - 120	80_{-0}^{+40}	100_{-60}^{+60}
h_0^{cry} (nm)	0 - 15	0_{-0}^{+0}	- -	0 - 30	10_{-5}^{+10}	- -
h_f^{cry} (nm)	20 - 100	55_{-5}^{+25}	65_{-6}^{+6}	60 - 110	70_{-10}^{+40}	95_{-23}^{+23}

root-mean-square deviation for each curve was calculated.

Table 2.3: Parameters used for the simulation of the RHEED integrated intensity and parameters extracted from the post-growth SEM images.

Parameter	Sample E		Sample F	
	Simulation	SEM	Simulation	SEM
ρ_{NW} (μm^{-2})	0.8	$0.76^{+0.13}_{-0.13}$	8.0	$8.4^{+2.1}_{-2.1}$
r_0^{NW} (nm)	12	- -	14	- -
$r_{f,b}^{NW}$ (nm)	20	20^{+2}_{-2}	27	27^{+2}_{-2}
$r_{f,t}^{NW}$ (nm)	23	23^{+2}_{-2}	27	27^{+2}_{-2}
h_f^{NW} (nm)	900	830^{+114}_{-114}	800	800^{+160}_{-160}
ρ_{cry} (μm^{-2})	0.4	$0.31^{+0.05}_{-0.05}$	6.0	$6.4^{+2.0}_{-2.0}$
r_0^{cry} (nm)	16	- -	14	- -
r_f^{cry} (nm)	100	95^{+66}_{-66}	80	80^{+30}_{-30}
h_0^{cry} (nm)	0	- -	0	- -
h_f^{cry} (nm)	100	95^{+40}_{40}	100	100^{+30}_{-30}

3 Absorption at different NW cross sections

Our interpretation of the transmitted and the diffracted electron intensities bases on the three aspects: NW radius, NW cross section and electron mean free path length. All these aspects are included in the mean scattering cross section $\Omega(r(k, t), \Lambda)$ of certain slices k of the NW. In this paragraph, we determine $\Omega(r(k, t), \Lambda)$ for different NW cross sections, namely hexagonal with two different orientations to the beam and a circular cross section. In analogy to figure 2 (a) and (b) in the main text, the different NW cross sections and the corresponding centre curves of the transmitted and diffracted intensities along x are depicted in figure 3.1. In figure 3.1(a) and 3.1(b), we depicted again for comparison, the case of a hexagonal NW cross section, where the electron beam is perpendicular to a side facet. In this geometry there exists always a non-zero intensity contribution at the outer edges of the NW. In the case of a hexagonal cross section, where the electron beam impinge at an edge, the intensity drops much faster and for larger radii the intensity tends to zero (figure 3.1(c) and 3.1(d)). NWs with circular cross section show an intermediate behaviour compared to the hexagonal cross sections for the centre curve (figure 3.1(e) and 3.1(f)). The decrease at the outer regions is much faster compare to figure 3.1(b), however there is still a contribution existing compared to 3.1(d).

In order to obtain the mean cross section $\Omega(r(k, t), \Lambda)$, we integrate the path distances of the electron beam in the NW $\gamma(x, k, t)$ along the NW diameter and consider additionally the attenuation of the electron beam intensity along $\gamma(x, k, t)$. In the following, we determine $\Omega(r(k, t), \Lambda)$ for the different NW cross sections shown in figure 3.1 and which then can be used in equation (5) in the main text to determine the diffracted intensity. For a hexagon where the electron beam is perpendicular to a side facet (figure 3.1(a)), $\gamma(x, k, t)$ can be written as:

$$\gamma(x, k, t) = \begin{cases} \sqrt{3}(r(k, t) + x), & \text{for } -r < x < -\frac{r}{2}. \\ \frac{\sqrt{3}}{2}r(k, t), & \text{for } -\frac{r}{2} \leq x \leq \frac{r}{2}. \\ \sqrt{3}(r(k, t) - x), & \text{for } \frac{r}{2} < x < r. \end{cases} \quad (3.1)$$

The integration along the NW diameter and the attenuation of the electron beam intensity along the path distance inside the NW result in $\Omega(r(k, t), \Lambda)$:

$$\begin{aligned}\Omega(r(k, t), \Lambda) &= \int_{-r(k, t)}^{r(k, t)} \int_0^{\gamma(x, k, t)} e^{-\frac{2\gamma(x, k, t)}{\Lambda}} dy dx \\ &= \frac{\Lambda^2}{\sqrt{3}} - \frac{1}{3} e^{-\frac{\sqrt{3} \cdot r(k, t)}{\Lambda}} \cdot \left(-3\sqrt{3} \cdot r(k, t)^2 + 3r(k, t)\Lambda + \sqrt{3}\Lambda^2 \right),\end{aligned}\quad (3.2)$$

In the second case, we calculate $\Omega(r(k, t), \Lambda)$ for a hexagon, where the electron beam is parallel to a side facet (figure 3.1(c)). Here $\gamma(x, k, t)$ is:

$$\gamma(x, k, t) = \begin{cases} \frac{1}{\sqrt{3}}x + r(k, t), & \text{for } -\frac{\sqrt{3}}{2}r \leq x \leq 0. \\ -\frac{1}{\sqrt{3}}x + r(k, t), & \text{for } 0 < x \leq \frac{\sqrt{3}}{2}r. \end{cases}\quad (3.3)$$

and $\Omega(r(k, t), \Lambda)$ is consequently

$$\Omega(r(k, t), \Lambda) = \int_{-\frac{\sqrt{3}}{2}r(k, t)}^{\frac{\sqrt{3}}{2}r(k, t)} \int_0^{\gamma(x, k, t)} e^{-\frac{2\gamma(x, k, t)}{\Lambda}} dy dx \quad (3.4)$$

$$= \sqrt{3}e^{-\frac{2r(k, t)}{\Lambda}} \Lambda(-2r(k, t) - \Lambda + e^{\frac{r(k, t)}{\Lambda}}(r(k, t) + \Lambda)). \quad (3.5)$$

The last case is a circular NW cross section, here $\gamma(x, k, t)$ and $\Omega(r(k, t), \Lambda)$ are:

$$\gamma(x, k, t) = \sqrt{r^2(k, t) - x^2} \quad (3.6)$$

$$\Omega(r(k, t), \Lambda) = \int_{-r(k, t)}^{r(k, t)} \int_0^{\gamma(x, k, t)} e^{-\frac{2\gamma(x, k, t)}{\Lambda}} dy dx \quad (3.7)$$

$$= \int_{-r(k, t)}^{r(k, t)} 2e^{-\frac{2\sqrt{r(k, t)^2 - y^2}}{\Lambda}} \sqrt{(r^2(k, t) - x^2)} dx. \quad (3.8)$$

For circular cross sections, an analytical formula does not exist. For further NW cross sections, $\Omega(r(k, t), \Lambda)$ can be determined accordingly.

The results can be found in figure 4 in the main text.

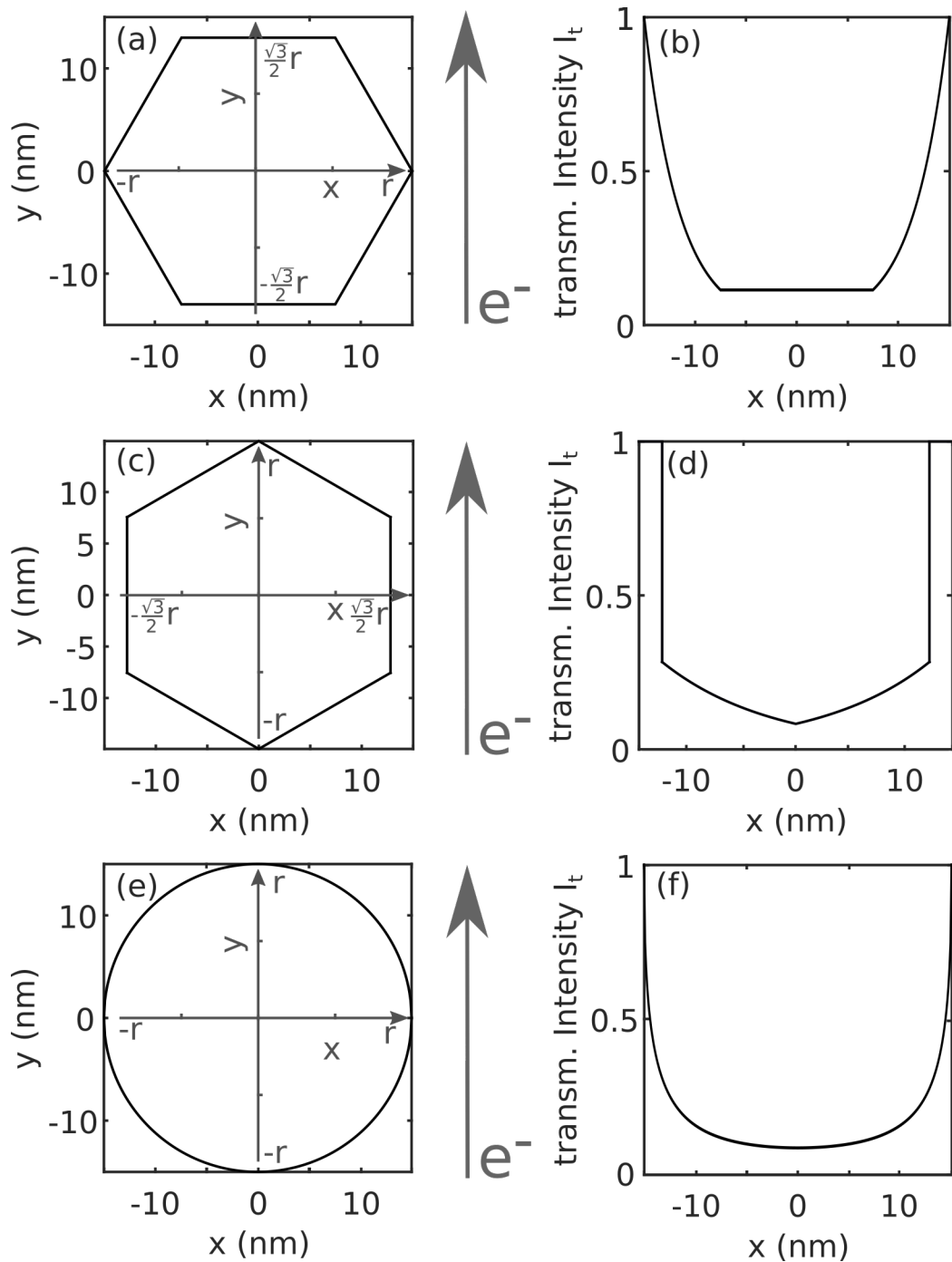


Figure 3.1: Different NW cross sections and their transmitted intensity with certain orientations to the electron beam direction. Here Λ is 12 nm.

4 The illumination height $\bar{\lambda}_{crit}$

In figure 4.1 (a) and 4.2 (a) the illumination height $\bar{\lambda}_{crit}$ is shown as function of the NW number density ρ_{NW} , the NW radius r^{NW} and the incidence angle of the electron beam α . In figure 4.1 (a) the incidence angle is kept constant at $\alpha = 0.6^\circ$ and in figure 4.2 (a) the NW radius is kept constant at $r^{NW} = 25$ nm. Both figures indicate that the NW number density ρ_{NW} is an important parameter for the illumination height $\bar{\lambda}_{crit}$, because with increasing number density, the distance between NWs decreases and thus the electron shadow covers more of the NWs. For a detailed analysis of the illumination height $\bar{\lambda}_{crit}$, we plotted selected profiles as a function of the NW number density ρ_{NW} in figure 4.1 (b) and figure 4.2 (b), as a function of the NW radius r^{NW} in figure 4.1 (c), and as a function of the incidence angle α of the electron beam in figure 4.2 (c).

By fitting the functions of the selected profiles by a power law functions, we can find a general expression for the final illumination height $\bar{\lambda}_{crit}$ in nm as a function of from α , r_f^{NW} and ρ_{NW} :

$$\bar{\lambda}_{crit} = \frac{c_1}{\rho_{NW}} \exp((c_2 \cdot \alpha)^{c_3} - (c_4 \cdot r_{NW})^{c_5}), \quad (4.1)$$

where α is given in rad, r_{NW} in nm and ρ_{NW} in nm^{-2} . The coefficients given by the results shown in figure 4.1 and 4.2 are $c_1 = 10^{-6} \text{ nm}^{-1}$, $c_2 = 2.8304 \cdot 10^6$, $c_3 = 0.1686$, $c_4 = 0.0574 \frac{1}{\text{nm}}$ and $c_5 = 0.4002$.

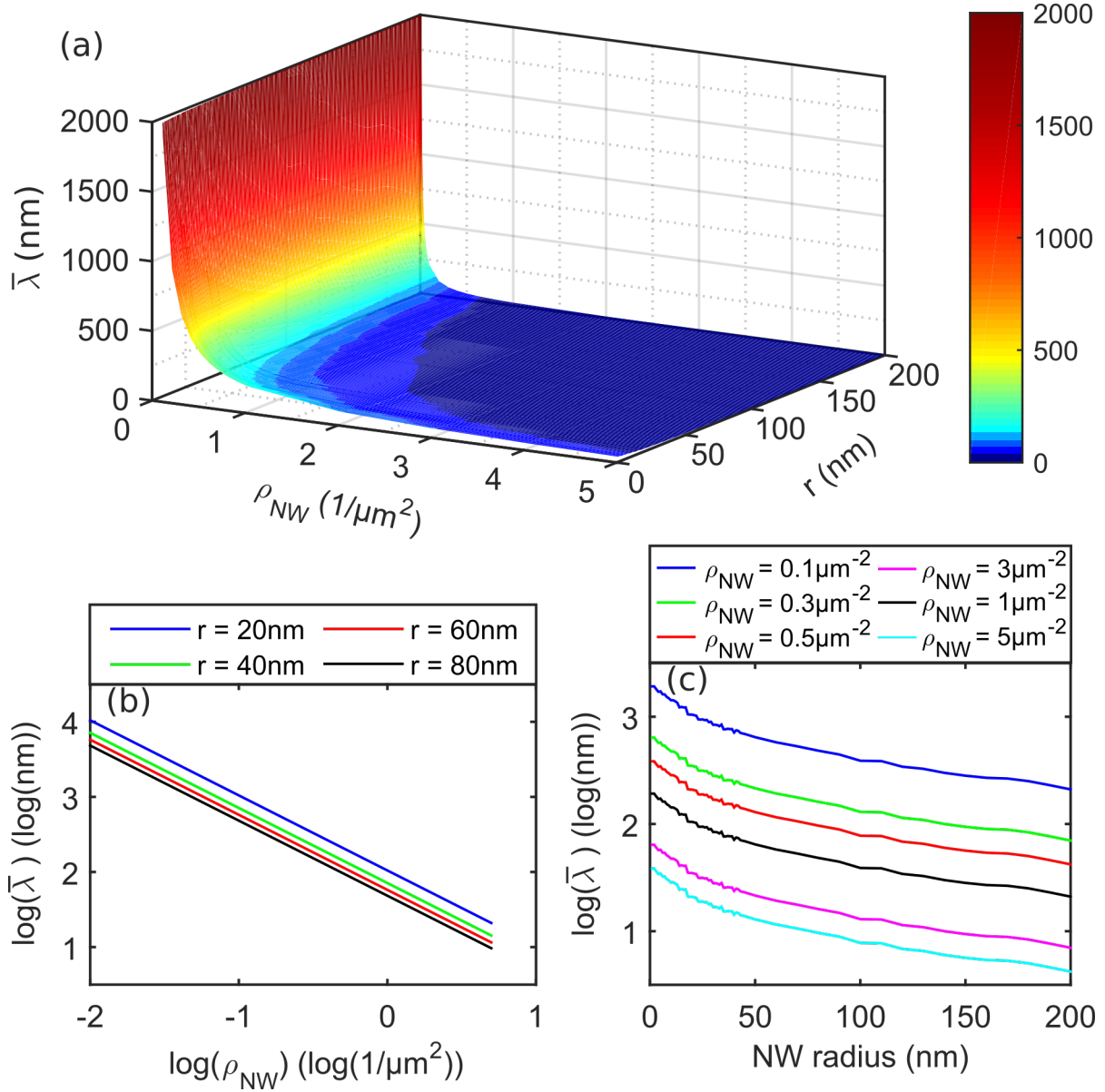


Figure 4.1: (a) Final illumination height $\bar{\lambda}_{crit}$ as function of NW density ρ_{NW} and r^{NW} at fixed angle $\alpha = 0.6^\circ$. (b) $\log(\bar{\lambda}_{crit})$ plotted vs. $\log(\rho_{NW})$ for different fixed r^{NW} . The slopes for the graphs are -1, indicating a hyperbola function. (c) $\log(\bar{\lambda}_{crit})$ plotted vs. r^{NW} for different fixed ρ_{NW} . The curves are only shifted in $\log(\bar{\lambda}_{crit})$ by changing ρ_{NW} .

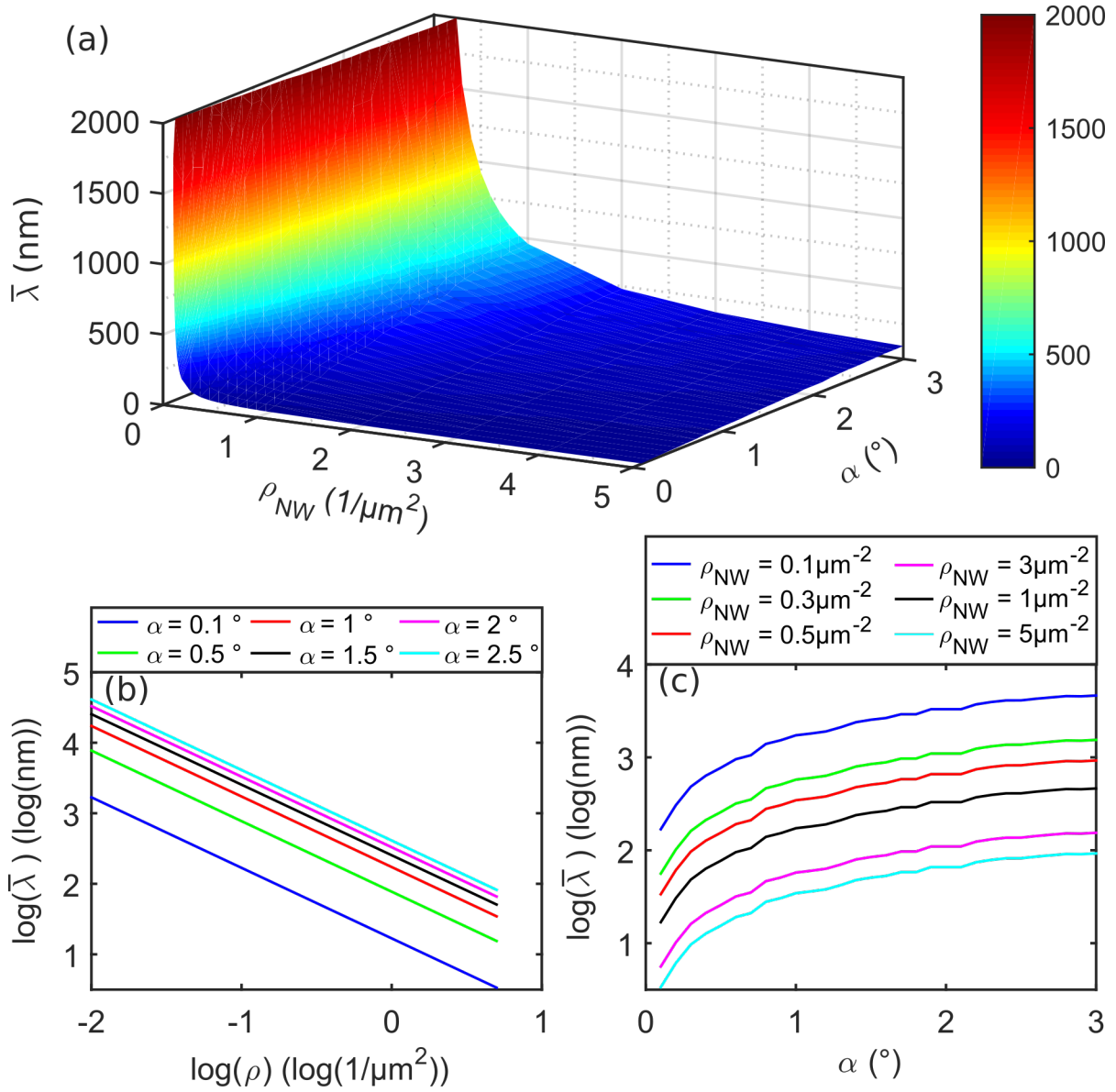


Figure 4.2: (a) Final illumination height $\bar{\lambda}_{crit}$ as function of NW density ρ_{NW} and angle α at fixed $r^{NW} = 25$ nm. (b) $\log(\bar{\lambda}_{crit})$ plotted vs. $\log(\rho_{NW})$ for different fixed α . The slopes for the graphs are -1, indicating a hyperbola function. (c) $\log(\bar{\lambda}_{crit})$ plotted vs. α for different fixed ρ_{NW} . The curves are only shifted in $\log(\bar{\lambda}_{crit})$ by changing ρ_{NW} .

Bibliography

- [1] SLOBODSKYY, T., SCHROTH, P., GRIGORIEV, D., MINKEVICH, A. A., HU, D. Z., SCHAADT, D. M., AND BAUMBACH, T. A portable molecular beam epitaxy system for in situ x-ray investigations at synchrotron beamlines. *Review of Scientific Instruments* 83, 10 (2012), 105112.
- [2] TAUCHNITZ, T., NURMAMYTOV, T., HÜBNER, R., ENGLER, M., FACSKO, S., SCHNEIDER, H., HELM, M., AND DIMAKIS, E. Decoupling the Two Roles of Ga Droplets in the Self-Catalyzed Growth of GaAs Nanowires on SiO_x/Si(111) Substrates. *Crystal Growth & Design* 17, 10 (2017), 5276–5282.